Frontiers in Bioscience Landmark

Front. Biosci. (Landmark Ed) **2022**; 27(5): 155
https://doi.org/10.31083/j.fbl2705155

Original Research

Atypical Extracellular Action Potentials from Posteromedial Hypothalamus in Anesthetized Humans

Jesús Pastor[1,2,*], Lorena Vega-Zelaya[1,2], Elena Martín-Abad[1,2,3]

[1]Clinical Neurophysiology, Hospital Universitario La Princesa, 28006 Madrid, Spain
[2]Fundación de Investigación Biomédica, Hospital Universitario La Princesa, 28006 Madrid, Spain
[3]PhD Program in Neuroscience, Autonoma de Madrid University-Cajal Institute, 28029 Madrid, Spain
*Correspondence: jesus.pastor@salud.madrid.org (Jesús Pastor)
Academic Editor: Graham Pawelec
Submitted: 9 February 2022 Revised: 16 April 2022 Accepted: 24 April 2022 Published: 12 May 2022

Abstract

Background: We obtained microelectrode recordings from four patients with intractable aggressivity who underwent surgery at posteromedial hypothalamus under general anaesthesia. We described two general types of extracellular action potentials (EAPs): typical/canonical and atypical. **Methods**: We analysed 337 units and 67 traces, which were characterized by the mean action potential (mAP). For the first phase, depolarization and repolarization, we computed amplitudes (V_{FP}, V_{Dep} and V_{Rep}) and durations (d_{FP}, d_{Dep} and d_{Rep}), maximum and minimum values of the first derivative (dV_{max}, dV_{min}), and amplitude and duration ratios. **Results**: Most of the canonical mAPs were positive (81.1%). EAPs with atypical mean action potentials (amAPs) were recorded in 42/337 cases. Only 35.6% of mAPs showed 2 phases. We identified the following types: N1P1N2 (38.3%), P1N1 (35.9%), amAP (12.5%), P1P2N1 (12.2%), N1P1 (4.7%), P1N1P2 (4.1%) and N1N2P1 (3.2%). We can define the properties of canonical forms as those units with (i) at least two opposite phases; (ii) $V_{Dep} \in [1.2, 2.7] \times |V_{Rep}|$ and strongly related by this function $V_{Rep} = -0.56\,(\pm 0.01)\,V_{Dep} - 1.83(\pm 0.79)$; (iii) a very strong relationship between dV_{max} and dV_{min}, given by the equation $dV_{min} = -0.91\,(\pm 0.03)\,dV_{max} - 0.37(\pm 0.12)$, both of which were included in the depolarization phase; (iv) related with V_{Dep} by the equation $dV_{max} = 0.08\,(\pm 0.001)\,V_{Dep} - 0.28(\pm 0.14)$; and (v) $d_{Dep} \sim 0.38 d_{Rep}$. However, the first phase does not pertain to the same dynamic process responsible for depolarization and repolarization. **Conclusions**: Atypical units are described here for the first time and are true EAPs that differ strikingly from canonical forms. To date, they have been observed only in the hypothalamus, but future research is needed to assess their existence in other brain structures.

Keywords: axons; capacitive current; deep brain stimulation; gap junctions; intractable aggressiveness; microelectrode recordings; sorting spikes

1. Introduction

Deep brain stimulation (DBS) has been demonstrated to be an effective surgical treatment for several movement disorders (e.g., Parkinson's disease, essential tremor, and dystonia) and appears to be promising for other pathologies, such as epilepsy, pain, major depression, and Alzheimer's disease. The process for all these diseases is to implant electrodes at different targets to modify the pathological activity in neural circuits by means of electrical stimulation. Microelectrode recording (MER) has long been known to be a reliable technique to identify neural structures [1].

One of these pathologies potentially treatable by DBS is intractable aggressivity, characterized by severe cases of unprovoked aggressive behaviour, usually associated with some degree of mental impairment and gross brain damage [2]. The aetiology can be due to genetic origin, perinatal insults, brain malformation, or posttraumatic, postencephalitic or epileptic seizures and is usually accompanied by self-aggressiveness, hyperkinesia, and destruction of objects. Patients usually need to be institutionalized and managed with major restraint measures. An early successful surgical treatment was posteromedial hypothalamomy [2,3]. Deep brain stimulation (DBS) of the posteromedial hypothalamus (PMH) has widely replaced ablative procedures because the clinical benefits appear to be similar, but the treatment can be titrated, is reversible, and has a low risk of complications [4–7].

The human hypothalamus is a complex structure composed of a number of groups of nuclei [8]. The identification of hypothalamic nuclei is particularly important to obtain good functional outcomes with DBS regarding optimizing battery life and decreasing secondary effects, especially considering that very sensitive nuclei related to arousal, circadian rhythms and hormone release are very close.

Most brain regions used for DBS have been described in terms of discharge patterns [9–16], but less attention has been devoted to the analysis of extracellular action potentials (EAPs), with the exception of the pedunculopontine nucleus [17,18] in a very limited way and some nuclei in the thalamus [19] and hypothalamus [20].

The hypothalamus is one of the least studied targets for DBS, probably because the pathologies treated with DBS in the hypothalamus have low prevalence. Descriptions of discharge patterns have been recently provided [21]. However,

it have been described, for the first time, features of EAPs from the posteromedial hypothalamus (PMH) and adjacent regions [20]. In that work, it was described for the first time a type of cell with a highly anomalous EAP morphology, which was referred to as atypical (i.e., atypical mean action potential or amAP). Notably, amAPs were found mainly in the PMH, with lower concentrations in the regions above or below the PMH.

The morphology of amAPs is not the only electrophysiological feature of this region that is difficult to explain, as amAPs can be indicated by the presence of negative EAPs or the existence of a first phase that precedes the depolarization phase.

In this study, we aimed to analyse the electrophysiological features of amAPs recorded from the hypothalamus in anaesthetized patients. A detailed description of conventional mAPs will be used as a cornerstone for comparisons to amAPs.

Acronyms have been enlisted in Abbreviations.

2. Materials and Methods

2.1 Patients

We studied 4 patients undergoing DBS treatment at PMH for intractable aggressivity (see Table 1 for clinical information).

2.2 Surgical Procedures

All the patients were operated on while under general anesthesia using propofol (5.48 $\pm$ 0.28 mg/kg/h, (4.5, 6.2)) and remifentanil (0.12 $\pm$ 0.02 μg/kg/min, (0.1, 0.2)), maintaining a bi-spectral index between 40 and 45. Neuromuscular blockade during intubation was accomplished with cis-atracurium (0.5 mg/kg).

The hypothalamus was identified using a 1.5 T magnetic resonance imaging (MRI, General Electric®, Fairfield, CT, USA), and the coordinates were located stereotactically with a neuronavigator (BrainLab®, Feldkirchen, Germany). The coordinates were calculated by fusing the MRI image and computed tomography scan according to the Schaltenbrand-Wahren map [22]. For hypothalamic DBS electrode placement, a tentative initial target was selected in the posterolateral hypothalamus according to the Sano's triangle (x = 2, y = 0, z = –2). All the coordinates (in mm) refer to the mid-intercommissural AC-PC line (anterior commissure-posterior commissure). Neuronal recordings (Leadpoint®, Minneapolis, MN, USA) were obtained beginning 10 mm above the target and progressing in steps of 0.5 mm. MERs (FHC®, Maine, USA) were obtained until 2 mm below the theoretical target. Impedance was always above 900 kΩ (1696 $\pm$ 80 kΩ, (900, 2900)).

MERs were obtained through 3–4 microelectrodes separated by 2 mm. A microdrive was fixed to a stereotactic Leksell Coordinate Frame (Elekta®, Stockholm, Sweden). The bandwidth for spontaneous activity was 200 Hz–5 kHz, with a sample rate of 24 kHz. The notch filter was off. PMH region was identified by MER and response to electrical stimulation [15,23]. After the PMH was identified, a quadripolar DBS electrode was implanted, with a programmable stimulator placed in an abdominal or pectoral location.

The reconstruction of the trajectory was described in detail elsewhere [24]. Anteroposterior and lateral coordinates were obtained from the post-op MRI performed one month after surgery. Using these points and the stereotactic angles, we reconstructed the real trajectory of the electrode in a three-dimensional space in 1-mm intervals.

2.3 Analysis of Extracellular Action Potentials

Data were exported as ASCII files, and analyses were performed off-line. The recordings spanned 30–90 s (72–216 $\times$ 10^4 points). Raw recordings were digitally filtered at bandwidth of 500 Hz–5 kHz using a 6th-order Butterworth. We tried other kind of filters (namely Chebysev and Bessel) with the same results. Considering that no synchronization analysis was done, we were not interested in differences between the phase response and finally decided by Butterworth that performs very well. We used zero-phase forward and reverse digital infinite impulse response filtering [25].

The polarity of the potentials was defined as positive (P) upward and negative (N) downward and was identified by order of appearance.

The algorithm has been described in detail elsewhere [19,20]. Briefly:

(1) EAPs must have two phases (depolarization and repolarization); therefore, we identified a tentative EAP when a positive/negative (P/N) phase was followed by a negative/positive (N/P) phase in a period of 0.25–0.65 ms. EAPs were defined as positive (P/|N| $>$1) or negative (P/|N| $<$1) according to the highest component identified.

(2) For every EAP, we measured the maximum (Vmax) and minimum voltages (Vmin, in μV), durations (in ms) of negative (dtN) and positive phases at half-amplitude (dtP), and maximum (dVmax) and minimum values of the first derivative (dVmin, in mV/s). These measures can be considered as a 6-dimension vector for every k-EAP, $EAP_k = \left\{V^k_{max}, V^k_{min}, dt^k_N, dt^k_P, dV^k_{max}, dV^k_{min}\right\}$.

(3) Construction of the mean action potential (mAP) from all the EAPs from the same cluster. A minimum of 10 EAPs was averaged. We identified hallmark points in mAPs. Every phase can be characterized by its polarity (P/N), duration and amplitude (V_i, i = 1, 2, 3).

To compare the structure of different kind of mAP we have considered features of the first phase, i.e., duration (d_{FP}) and absolute value of amplitude ($|V_{FP}|$), the depolarization phase, i.e., duration (d_{Dep}) and amplitude (V_{Dep}), the repolarization phase, i.e., duration (d_{Rep}) and amplitude (V_{Rep}), maximum and minimum values of the first derivative (dV_{max} and dV_{min}, respectively) and total duration (d_{mAP}) and amplitude (V_{mAP}) of mAP. Mean frequency

Table 1. Demographic and clinical findings.

Patient	Age (yrs)	Sex	Intellectual capacity	Medical history	Medication	MRI
1	22	F	severe mental retardation	cluster headache, epilepsy	TPM, CLZ, RIS, LVM, OLZ	moderate diffuse cortico-subcortical atrophy; pineal cyst
2	22	M	moderate mental retardation	perinatal hypoxia	GBP, VPA, CYP, Li, OLZ	normal
3	48	M	moderate mental retardation	OCD, AVM, complex partial seizure	CBM, GBP, ZPX, CTP, CLZ	extensive encephalomalacia in right temporal lobe
4	37	F	severe mental retardation	epilepsy	LVM, OLZ, TPM, RIS, ARP	normal

ARP, arpiprazole; AVM, arterio-venous malformation; CBM, carbamacepine; CLZ, clorazepate; CTP, citalopram; CYP, cyproterone; GBP, gabapentine; Li, lithium; LVM, levomepromazine; MRI, magnetic resonance imaging; OCD, obsessive-compulsive disorder; OLZ, olanzapine; RIS, risperidone; TPM, topiramate; VPA, valproic acid; ZPX, zuclopenthixol.

for every neuron (Freq, in Hz) was obtained from the inverse of the instant period.

We have built amplitude and duration ratios to characterize canonical forms of mAP. So, we have $|V_{FP}/V_{Dep}|$, $|V_{Dep}/V_{Rep}|$, $|V_{FP}/V_{Rep}|$, d_{FP}/d_{Dep}, d_{FP}/d_{Rep} and d_{Dep}/d_{Rep}.

All analyses were performed in homemade MATLAB®R2018 (Natick, MA, USA) scripts.

2.4 Statistics

Kurtosis (K) was computed for every group, and only values between 2 and 8 were acceptable for the homogeneous group [26]. Extreme outliers were removed. Statistical analysis was applied only to these groups.

Statistical comparisons between groups were performed using the Mann-Whitney U test or Kruskal-Wallis one-way ANOVA on ranks if normality failed. In the last case, Dunn's method was used for all pairwise post hoc comparisons. Normality was evaluated using the Kolmogorov-Smirnov test. Chi-square test (χ^2) was used to assess the difference between groups, The independence of variables (e.g., peak-to-peak action potential amplitude and amplitudes of depolarizing and repolarizing phases) was assessed by computing the rank (rnk) for the matrix containing observations (n) in rows and variables (p) in columns. Therefore, if rnk $<p$ (considering that n $>p$ always), then there would be some dependent variable that could be removed. However, when rnk = p, all the variables are independent and must be included in the analysis.

Pearson's correlation coefficient was used to study linear dependence between variables. Linear regression significance was evaluated by means a contrast hypothesis against the null hypothesis $\rho = 0$ using the formula

$$t = \frac{r\sqrt{n-2}}{\sqrt{1-r^2}}$$

This describes a t-Student distribution with n-2 freedom degrees [27].

SigmaStat® 3.5 software (Point Richmond, CA, USA) and MATLAB were used for statistical analyses.

The significance level was set at $p = 0.05$, and the results are shown as the mean $\pm$ standard error of mean (SEM). In several cases, for clarity, also median and interpercentile range 10–90 -IP_{10-90}, (between brackets) will be shown.

3. Results

We analysed traces from 9 consecutive locations spanning 4.0 mm from 7 trajectories. Overall, we analysed 337 units and 67 raw traces. Given that each mAP was composed of 34.8 $\pm$ 10.6 APs, the total number of unitary APs analysed was 11,700.

3.1 Types of Extracellular Action Potentials

Similar to thalamus recordings, in the hypothalamus, most mAPs were characterized by the following features: (i) a higher amplitude positive/negative phase followed by (ii) a phase of the opposite polarity, and (iii) the first phase was shorter and included the dV_{max} and dV_{min} values, and (iv) the later phase was clearly longer (Fig. 1A,B). The first phase was assumed to be depolarization, while the second was assumed to be repolarization [19]. We also found that most mAPs had an initial small and short phase, prior to depolarization, which was either positive or negative and could be interpreted as postsynaptic potentials, although this has not yet been conclusively demonstrated.

We more deeply analysed the structure of the mAPs, defined as the arrangement of the components composing each of the waveforms [20]. Excluding atypical mAPs (amAPs), most of the mAPs were positive, 260/295 (81.1%), and fewer were negative, 25/290 (19.9%). Atypical mAPs were recorded in 42/337 cases (12.5%). Most of these atypical waveforms were positive, but in other cases, the polarity was difficult to identify. Moreover, they presented structures clearly different from the other conventional types. Negative mAPs were recorded simultaneously with positive ones. Usually, the mAP had more than two phases. Only 120/337 (35.6%) mAPs showed 2 phases. On the other hand, a more frequent occurrence was to observe either a small positive or negative deflection before the main component, which resulted in a three-

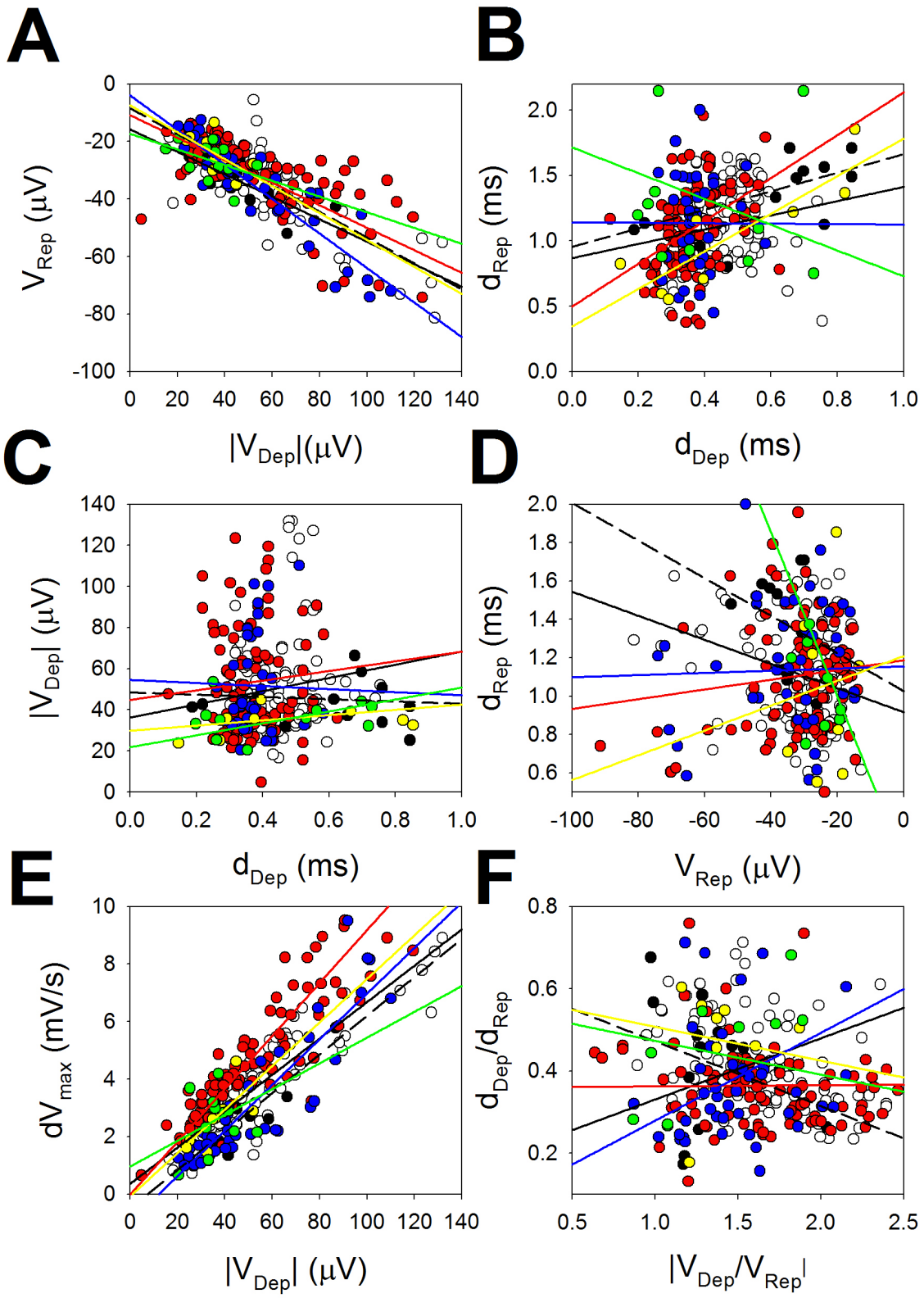

Fig. 1. Correlations between pairs of variables. (A) V_{Dep} vs V_{Rep}. (B) d_{Dep} vs d_{Rep}. (C) d_{Dep} vs V_{Dep}. (D) V_{Rep} vs d_{Rep}. (E) V_{Dep} vs dV_{max}. (F) $|V_{Dep}/V_{Rep}|$ vs d_{Dep}/d_{Rep}. P1N1 = white dots and black regression lines; V_{Dep} and V_{Rep} for N1P1, N1N2P1 and P1N1P2 mAPs were multiplied by -1 to preserve coherence with positive cells. N1P1 = empty dots and black lines; P1N1 = black dots and black dashed lines; N1PN2 = red dots and lines; P1P2N1 = blue dots and lines; N1N2P1 = yellow dots and lines; and P1N1P2 = green dots and lines.

phase structure. In 113/337 (38.3%) cases, an N1P1N2 structure was observed, followed in 106/337 (35.9%) cases with a P1N1 structure, and a P1P2N1 structure in 41/337 (12.2%), an amAP in 42/337 (12.5%), an N1P1 structure in 14/337 (4.7%), an P1N1P2 structure in 12/337 (4.1%), and an N1N2P1 structure in 9/337 (3.1%) cases.

3.2 Features of Canonical Forms

Theoretical considerations and empirical facts show that canonical forms of action potentials are composed of a high depolarization phase followed by a repolarization phase. Considering that both phases are part of the same process [28–30], a high correlation between them would be expected. The maximum and minimum values of the first derivative were located during the rising and falling periods of the depolarizing phase, respectively.

We plotted linear correlations between the different variables describing the P1N1 (n = 106), N1P1 (n = 14), N1P1N2 (n = 113), P1P2N1 (n = 41), N1N2P1 (9) and P1N1P2 (n = 12) cells in Fig. 1. We have added a new figure at Appendix (Appendix Fig. 7) to show the network for every kind of mAPs. Surprisingly, practically no correlations were observed between the durations of the phases or the durations and amplitudes (except for P1N1).

All the cells showed a strong relationship between V_{Dep} and V_{Rep} and between V_{Dep} and dV_{max}. Moreover, the slopes of the regression lines for both pairs were similar. Consequently, these properties can be used to differentiate between typical and atypical mAPs.

We assessed these relationships as amplitude and duration ratios. We show these ratios to identify constant relationships between cells. In Fig. 2, we compare the amplitude and duration ratios for all typical cells. Considering all the pairs between each kind of mAP and each ratio, we have $4 \times C_2^4 + 2 \times C_2^6 = 54$ possibilities (C indicates combinations). However, we observed significant differences (post hoc Dunn's test for ANOVA on ranks) only for the V_{FP}/V_{Dep} and V_{FP}/V_{Rep} ratios for the pair of P1P2N1 and N1N2P1 cells, where the first phase had an opposite polarity.

Therefore, these ratios can be considered nearly constant for different kinds of cells. It is quite interesting to observe that although no correlations between pairs d_{Dep} and d_{Rep} were obtained (Fig. 1B), the ratio d_{Dep}/d_{Rep} can be considered nearly constant, with a value of 0.38 ± 0.01 (median and IP_{10-90}: 0.37 (0.25, 0.57)).

With these results, we defined the properties of cells considered canonical as those cells with (i) at least two opposite phases, with the higher, which is always the first of the two, considered depolarization, followed by a repolarizing phase; (ii) $V_{Dep} \in [1.2, 2.7] \times |V_{Rep}|$ and strongly related by the function $V_{Rep} = -0.56\,(\pm 0.01)\,V_{Dep} - 1.83(\pm 0.79)$; (iii) a very strong relationship between dV_{max} and dV_{min} given by the equation $dV_{min} = -0.91\,(\pm 0.03)\,dV_{max} - 0.37(\pm 0.12)$, both of which were included in the depolarizing phase; (iv) a relationship with V_{Dep} by the equation $dV_{max} = 0.08\,(\pm 0.001)\,V_{Dep} - 0.28(\pm 0.14)$; and (v) $d_{Dep} \sim 0.38 d_{Rep}$.

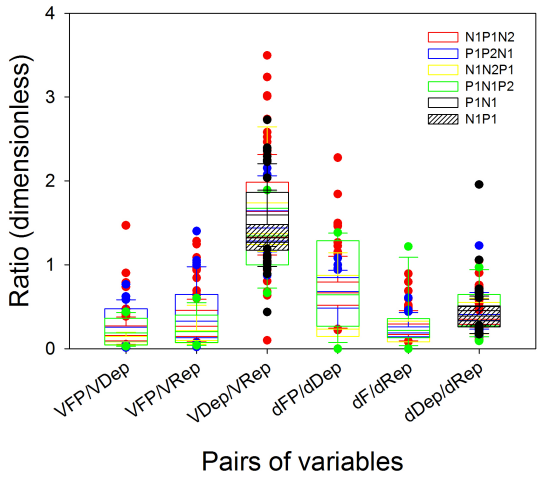

Fig. 2. Amplitude and duration ratios for all the typical mAPs. No differences were observed for ANOVA on ranks, with the exceptions of the V_{FP}/V_{Dep} and V_{FP}/V_{Rep} for the pair of P1P2N1 (blue) and N1N2P1 (yellow) cells.

Nevertheless, most of the recorded cells (74.4%) showed an initial phase prior to the depolarization phase. For all of these cells, the 5 conditions stated above were applicable, and therefore, these cells can be included as typical or canonical cells. We analysed the different correlations between pairs of magnitudes affecting the first phase (Fig. 3) and other properties of the APs. However, none of these correlations were significant.

Therefore, there were no correlations between FP and variables characterizing the depolarization or repolarization phases. Moreover, the coefficients of variation ($SEM/\bar{x}$) were $|V_{FP}/V_{Dep}| = 0.08$, $|V_{FP}/V_{Rep}| = 0.08$ and only 0.01 for $|V_{Dep}/V_{Rep}|$; the same measure for the duration ratios d_{FP}/d_{Dep}, d_{FP}/d_{Rep} and d_{Dep}/d_{Rep} were 0.11, 0.11 and 0.03 respectively, which implied that the variation was higher for ratios involving the FP.

These data suggest that the first phase was not associated with the same dynamic process of action potentials responsible for depolarization and repolarization.

3.3 Features of Atypical Forms

As previously stated, up to 12.5% of cases were amAPs, a percentage that cannot be considered anecdotal. Besides, this kind of cells was recorded from all the patients. As with the canonical cells, we considered depolarization as the phase where dV_{max} and dV_{min} occur. In Fig. 4 we have showed the canonical mAPs (upper row) and its atypical counterparts (lower row) for clarification.

The observed amAPs have been named wide P1N1 (wP1N1, Fig. 4E) cells, cells with a last phase (N1P1NLF,

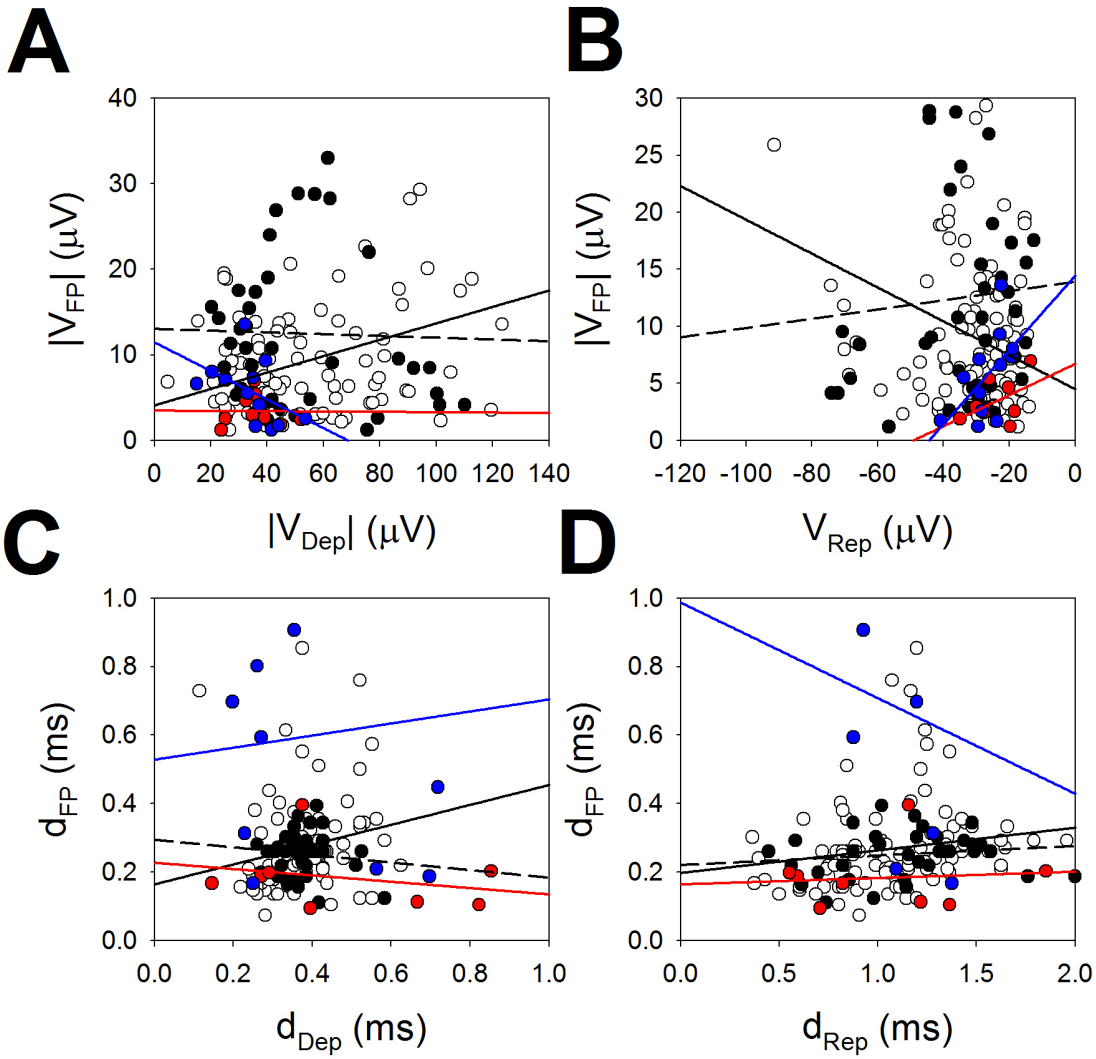

Fig. 3. Correlations between the FP variable and other variables. (A) V_{Dep} vs. V_{FP}. (B) V_{Rep} vs. V_{FP}. (C) d_{Dep} vs. d_{FP}. (D) d_{Rep} vs. d_{FP}. V_{Dep} and V_{Rep} for N1N2P1 and P1N1P2 mAPs were multiplied by -1 to preserve coherence with positive cells, and the amplitude of the first phase was $|V_{FP}|$. N1PN2 = empty dots and black lines; P1P2N1 = black dots and black dashed lines; P1P2N1 = red dots and lines; N1N2P1 = blue dots and lines.

Fig. 4F), and positive bimodal (PbiN1, Fig. 4G) and negative bimodal (NbiP1, Fig. 4H) cells. Each type of cell is plotted below its canonical cell counterpart to clarify the difference. Explicitly, wP1N1 cells (2/42, 5%) have a longer d_{Dep} than P1N1 cells. N1P1NLF cells (27/42, 64%) show an initial negative phase with dV_{max} and dV_{min}; therefore, this pattern could be considered a depolarization phase followed by a repolarization phase and by a third negative phase smaller than the first, referred to as the last phase. PbiN1 cells (12/42, 29%) are characterized by the presence of two positive waves of similar amplitude; in fact, dV_{max} is included in the first wave, in contrast to P1P2N1 cells, where dV_{max} is located in the second positive wave (Fig. 4C). Finally, NbiP1 cells (1/42, 2%) are similar to PbiN1 cells but with opposite polarity.

The first aspect we had to assess with respect to these amAPs was the possibility that such strange morphologies would arise from an erroneous sorting method that mixed different canonical forms. Therefore, it was extremely important to show atypical cells obtained from raw records. Fig. 5 shows three examples of amAPs obtained directly from the raw records before any sorting process.

Therefore, it can be concluded that amAPs are truly extracellular action potentials and were not artificially constructed. In this sense, the amplitude and duration ratios of the amAPs were quite different from those of the canonical mAPs . From a total of 14 ratios, in 10 cases, a significant difference was observed (71%); a difference was observed with 6/7 amplitude ratios (86%), with the only exception being V_{Dep}/V_{Rep} for the pair of P1N1 and wP1N2 cells, while the difference was observed with 4/7 (57%) duration ratios.

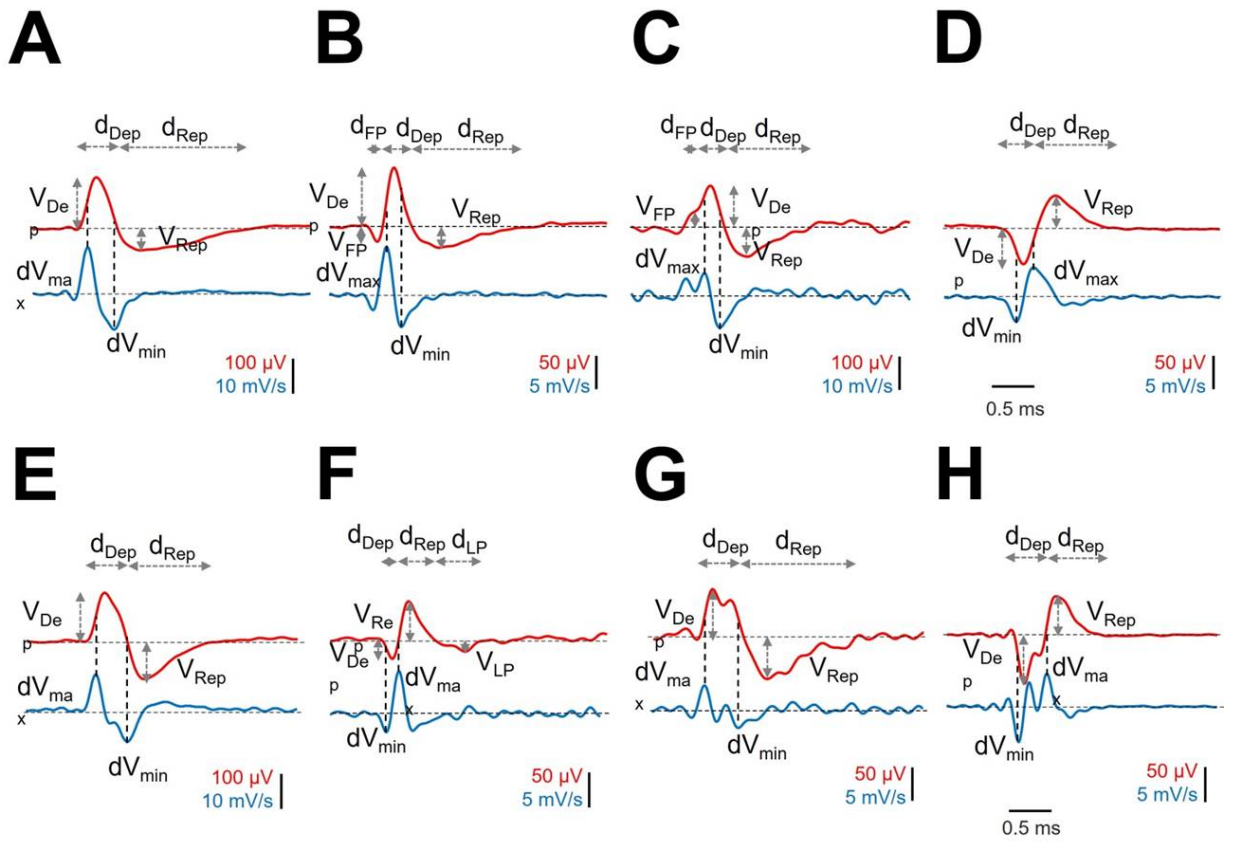

Fig. 4. Different phases of mAPs (red lines) and relationships with the first derivative (blue lines) for canonical and atypical cells. (A) P1N1 (B) N1P1N2 (C) P1P2N1 to (D) N1P1 cells for comparison with atypical cells in (E) wP1N1 (F) N1P1NLF (G) PbiN1 and (H) NbiP1. Horizontal dashed arrows indicate periods, and vertical dashed arrows indicate amplitudes of phases. Black dashed lines mark the maximum and minimum values of the first derivatives.

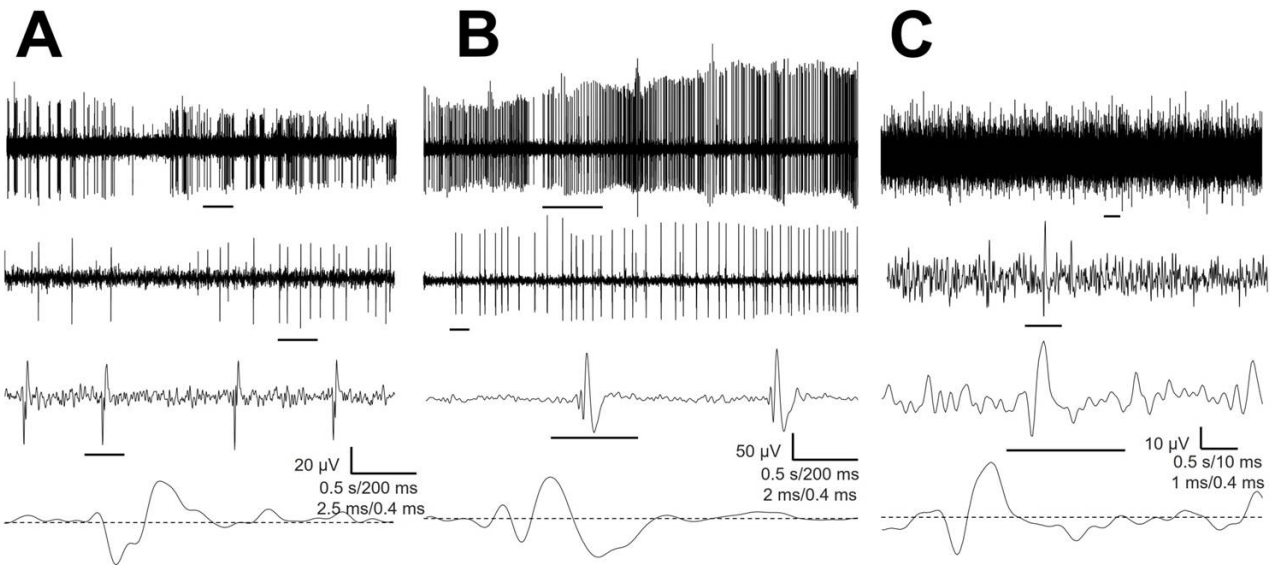

Fig. 5. Atypical extracellular action potentials recorded directly from the raw records before sorting. (A) NbiP1 (B) PbiN1 and (C) N1P1NLF. The horizontal lines under each record are expanded in the bottom panels. The horizontal calibration bar for every column corresponds from the upper to the lower row.

The structures of atypical PbiN1, NbiP1 and wN1P1 cells suggested a composition of simple mAPs. In fact, a summation of two P1N1 cells delayed by 0.20–0.24 ms resulted in mAP quite similar to PbiN1 and wP1N1 (Fig. 6B,C). The same process using two consecutive N1P1 cells gave rise to a structure highly similar to NbiP1 (Fig. 6D).

Unfortunately, we had no hypothesis about the sources leading to N1P1NLP cells, which are the most frequent amAPs.

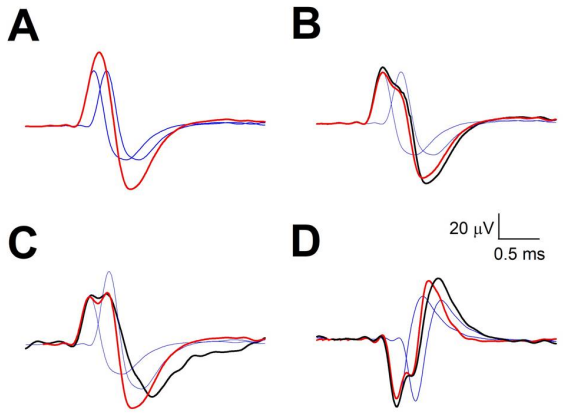

Fig. 6. Composition of atypical mAPs from simple cells. (A) Theoretical cell (not actually recorded) with a delay between unitary mAPs = 0.16 ms (B) wP1N1, delay = 0.21 ms (C) PbiN1, delay = 0.24 ms (D) NbiP1, delay = 0.24 ms. Blue = true unitary mAPs at different delays; red = theoretical mAPs formed by combining the two unitary mAPs; black = recorded amAP.

4. Discussion

To the best of our knowledge, this is the first study describing in detail the features of the atypical structure of EAPs in the human brain and, specifically, in the hypothalamus.

Recently, it has been shown that the types of mAPs in the hypothalamus are similar to those described in the thalamus [19,20], with the majority of cells showing three phases. Despite the similar morphology in both brain structures, the properties of the mAPs were different, showing that mAP morphology is region specific. However, in the thalamus, we did not record the amAPs that were recorded in the hypothalamus [20]. This fact adds another element of regional specificity regarding the structure of action potentials. EAPs can provide information about several properties of intracellularly recorded action potentials [28,29]; therefore, the MER goal should not exclusively consider EAPs as binary events (present/absent). To date, scarce attention has been devoted to the analysis of EAPs. In fact, only EAP width has been reported from recordings in the pedunculopontine nucleus in humans, and a bimodal distribution has been observed with a longer APs attributed to cholinergic neurons and shorter APs attributed to glutamatergic transmission [18,30,31]. However, no other properties have been analysed (number of phases, features of phases, derivatives, etc.) until our previous studies in thalamic nuclei [19] and hypothalamic nuclei [20].

We have analysed in detail the structure of canonical forms of mAPs in the hypothalamus, and we have identified five features defining conventional or canonical mAPs. These properties can be well fitted to the described basis of neuronal excitability *in vivo* by means of quantitative methods [32–35]. The tight relationship between V_{Dep} and V_{Rep} and dV_{max} demonstrates that the three variables are components of the same dynamic process, as can be expected. In contrast, the absence of a correlation between durations was not as expected. Nevertheless, as we have shown in Additional materials (Appendix Figs. 8,9), the different orders of magnitude for voltages (82.2 ± 2.4 (69.3 [49.2, 130.2] μV)) and durations (1.66 ± 0.03 (1.63 [1.2, 2.2]) ms) makes the duration measures much more sensitive to noise (see Appendix). Most likely, the smaller amplitude of hypothalamic cells relative to the thalamus precludes a better correlation between d_{Dep} and d_{Rep}.

The ratios of amplitudes and durations for the several phases of the canonical forms have been proven to be a robust way to characterize typical mAPs. It is quite interesting to observe that different types of mAPs share similar values of V_{Dep}/V_{Rep} or d_{Dep}/d_{Rep}, even when no good correlation was obtained. These quasi-constant ratios endorse the unity of the dynamic system responsible for mAPs.

The shape of the EAP is similar and proportional to the total transmembrane current from the perisomatic region [28]. However, as we previously described in the thalamus [19] and hypothalamus [20], most cells have a small phase before depolarization. This first phase can be observed with either positive or negative polarities. Given that quantitative and experimental data have shown the presence of capacitive current prior to the large depolarizing phase, this origin could be hypothesized for the first phase described here. However, capacitive current is elicited by current spreading to dendrites from the soma and is always of the opposite polarity as depolarization; therefore, we would obtain only N1P1N2 and P1N1P2 types. Thus, capacitive current cannot explain cells such as P1P2N1 (12.2%) and N1N2P1 (3.1%). Moreover, the magnitude of this current is between 10 and 50 times lower than the perisomatic current and cannot explain the amplitude and duration of the FP described here. Another possibility could be that the first phase is related to postsynaptic potentials, which can explain the difference in polarity. This possibility is reinforced by the lack of correlation and the greater variance for V_{FP} and d_{FP} and other phases of EAPs. If this phase is related to the process of APs, we should expect a greater correlation, as described for V_{Dep} and V_{Rep}, although perhaps

not for d_{FP}. In addition, we should expect values for amplitudes and duration ratios closer to those recorded in the depolarization and repolarization phases, but we truly found a variation in these ratios between 4 to 8 times greater than for ratios involving depolarization and repolarization. Another reason to consider the first phase as having a synaptic origin is the different features described in the thalamus [20]. A different morphology of the dendritic tree and the density and kind of receptors could give rise to different morphologies of postsynaptic potentials. A comparison with awake patients could shed light on this possibility because we can postulate similar features for action potential dynamics but some changes in the characteristics of synaptic activity. Although we cannot be sure whether synaptic potentials are the origin for the first phase, we can practically exclude its belonging to the dynamic system from which the EAP originates.

Another possibility to explain N1P1N2 cell morphology to capacitive or synaptic activity could be consider these kinds of cells as EAPs originating from axons, not the perisomatic region. Referential recordings from nonmyelinated fibres result in waveforms quite similar to a smaller first negative phase, followed by a higher positive and finally a third negative longer phase [36]. If this kind of mAP would be, in fact, in axons, it could be expected that its percentage would be greater in regions richer in white fibres, such as the hypothalamus (i.e., caudate-pallidal fibres and lenticular, tuberomamillar and dorsal longitudinal fascicles go through the hypothalamus), and lower in nuclei mainly composed of dendrite-soma structures, such as the basal ganglia [8]. This was true, because in the thalamus, the percentage of N1P1N2 was 19.4% (216/1114 cells), while in the hypothalamus, this percentage was nearly double (37.6%, 53/141 cells) [20]. In fact, the initial axon segment is the dominant contributor to the extracellular action potentials of cultured neurons [37].

As previously described in the thalamus, negative mAPs have also been described in the hypothalamus. Absolute values of amplitude and duration for repolarization (what we to consider as the negative phase) are similar to repolarization in positive cells. If depolarization originates from the transmembrane current going into the cell [35,38], we should think that negative depolarization originates from the transmembrane current coming from inside the cell. However, this case has not been described to date. The presence of these negative cells is high enough to discard an anecdotal finding; therefore, the transmembrane sources of current for these cells remain to be explained. In animal cortical recordings, a high amplitude positive action potential different from conventional negative spikes has been described, and the features of both types of spikes, such as amplitude and duration, were clearly different [39]. However, these findings were not observed in our case, where the properties of the positive and negative mAPs (absolute magnitudes for amplitudes and phase durations) were on the same order of magnitude.

To the best of our knowledge, this is the first description of EAPs that significantly differs from that conventionally described in animals and humans or quantitatively predicted [32,34,40]. First, it is important to keep in mind that despite their anomalous structure, they are real action potentials and not artefacts from erroneous sorting. Although we have denominated the amAPs in a similar way to canonical forms, the amplitudes and durations are strikingly different. The amAPs PbiN1 and NbiP1 have three well-defined phases. However, the first phase cannot be considered a canonical first phase because it is usually the higher amplitude phase. Obviously, neither a postsynaptic potential nor capacitive current can be so high. In fact, both dV_{max} and dV_{min} are placed inside the complex structure formed by the first two phases. Along with the high amplitude, as high as the V_{Dep}, these facts suggest that the biphasic structure can be explained as two consecutive simple EAPs. In fact, the composition of two canonical P1N1 and N1P1 EAPs delayed between 0.16 and 0.24 ms reproduced the main features of PbiN1, wP1N1 and NbiP1. Therefore, consecutive canonical spikes separated by less than ¼ ms could explain these types of atypical cells. Synaptic communication takes an approximately 1-ms delay in addition to the time for travel along the axon [32,33]. Therefore, even for very closely placed neurons, we can exclude synaptic mediation for a consecutive pair of spikes at this short delay, although we cannot exclude that both cells would be driven by a third cell. On the other hand, the refractory period excludes the possibility of a second spike from the same neuron. Therefore, one possibility to explain consecutive spikes from different neurons at such a short delay would be ephaptic communication or gap junctions (GJs). Connexins are expressed by grey but not white matter astrocytes [41]; they are important for the developing cortex [42] and are ubiquitous in the cortex between fast-spiking parvalbumin-positive interneurons and interneuron-neurons [43], although their presence in pyramidal cells from the adult cortex is still debated. Evidently, we cannot probe the presence of GJs in the human hypothalamus with these results, and further studies are needed, but it is an interesting suggestion.

Another possibility to explain the broad mAP could be the participation of calcium currents. It is well known that this type of conductance enlarges the duration of action potentials and can be located at dendritic sites [44].

The most frequently found amAP was N1P1N2LP. Although slightly similar at first sight to N1P1N2 canonical cells, there were some differences. For the canonical mAP, the ratio V_{FP}/V_{Rep} was 0.32 ± 0.2, and for the amAP, it was 6.77 ± 2.63, indicating that phase N1 was a true first phase, but for the amAP, it was not. In fact, the maximum values for the first derivate, which in canonical forms are inside the depolarization phase, were located in the N1 phase in this atypical cell, suggesting that this waveform is in fact

the depolarization phase. If this was true, the $V_{Rep} > V_{Dep}$, which is another anomaly. However, the volume conduction theory could explain this amAP as an EAP generated by axons, as we discussed in relation to N1P1N2 cells (see above) [36]. In fact, the different distances from the active electrode to the source could be the explanation for both kinds of waveforms. If this were true, regions with a higher density of nonmyelinated fibres would be more prone to show both types of mAPs, as we have recorded from the hypothalamus.

Nevertheless, it is important to understand that our data were obtained from a small number of patients. Although these data seem to be robust, a larger cohort study is needed to corroborate our interpretation of various EAP patterns as atypical and to confirm a connection between the presence of atypical potentials and the target identification. To further corroborate our interpretations of the EAP, simulations with neural models incorporating ion channel dynamics could be helpful.

5. Conclusions

EAPs of hypothalamic cells in anaesthetized humans can be divided into canonical forms, sharing a set of properties that are highly robust, mainly concerning the relationship between V_{Dep} and V_{Rep}. These cells show a three-phase structure in the majority of cases. However, there is another type of EAP that clearly differs from canonical. These atypical cells represent 12.5% of cells and clearly show different morphologies. To date, these atypical cells have been described only in the hypothalamus, although more research is needed to ascertain their presence in different brain regions.

Script Availability Statement

The MATLAB® script is available upon request from corresponding author.

Abbreviations

amAP, Atypical Mean Action Potential; AP, Action Potential; DBS, Deep Brain Stimulation; d_{mAP}, Duration of the mean Action Potential; dtN/dtP, Duration of Negative/Positive phases at half-amplitude of EAP; d_{Dep}, Duration of the Depolarization; d_{FP}, Duration of the First Phase; d_{Rep}, Duration of the Repolarization; dV_{max}/dV_{min}, Maximum/Minimum values of the first derivative; EAP, Extracellular Action Potential; Freq, Frequency of the raw trace; GJs, Gap junctions; ISI, Inter-Stimulus Interval; MER, Microelectrode Recording; mAP, Mean Action Potential; MRI, Magnetic Resonance Imaging; NbiP1, Negative bimodal (Dep) positive (Rep) phases cell; N1P1, Negative (Dep) and Positive (Rep) phases cell; N1P1N1, Negative (FP), Positive (Dep) and Negative (Rep) phases cell; N1P1NLF, Negative, Positive and Negative Last-Phase cell; N1N2P1, Negative (FP), Negative (Dep) and Positive (Rep) phases cell; PI, Pause Index; PR, Pause Ratio; PS, Power Spectra; P/N, Positive/Negative phase; P1N1, Positive (Dep) and Negative (Rep) phases cell; P1P2N1, Positive (FP), Positive (Dep) and Negative (Rep) phases cell; P1N1P2, Positive (FP), Negative (Dep) and Positive (Rep) phases cell; rnk, Rank for the matrix containing observations; SW, Schaltenbrand-Wahren; PbiN1, Positive bimodal (Dep) and negative (Rep) cells; PMH, Posteromedial Hypothalamus; $V_{AP\pm}$, Positive/negative voltage thresholds of mAP; V_{Dep}, Amplitude (voltage) of the Depolarization phase; V_{FP}, Amplitude (voltage) of the First Phase; V_{mAP}, Amplitude (voltage) of the mean Action Potential; V_{max}/V_{min}, Maximum/Minimum voltages of EAP; V_{Rep}, Amplitude (voltage) of the Repolarization phase; $V\pm$, Maximum/minimum voltage threshold; wP1N1, Wide Positive (Dep) and Negative (Rep) phases cell.

Author Contributions

JP is responsible of the idea. LV-Z and EM-A participated in data collection. JP developed the analytical methods and EM-A and LV-Z participated also in analysis and interpretation, and JP was responsible for manuscript preparation. All authors have approved the submitted version of this manuscript.

Ethics Approval and Consent to Participate

The experimental procedure was approved by the medical ethics review board of the Hospital Universitario de La Princesa and was deemed “care as usual”. Under these circumstances, written informed consent was not required because all procedures were done by clinical necessity and analysis was off-line. The study was accomplished according to standards for human research and in accordance with the Helsinki Declaration.

Acknowledgment

Authors want to acknowledge the collaboration during surgeries of neurosurgeons Marta Navas and Cristina Torres and anaesthesiologists María Luisa Meilán and Eva de Dios and Angel Nuñez by its comments during the elaboration of the manuscript.

Funding

This research received no external funding.

Conflict of Interest

The authors declare no conflict of interest. JP and LV-Z are serving as the guest editor of this journal. We declare that JP and LV-Z had no involvement in the peer review of this article and has no access to information regarding its peer review. Full responsibility for the editorial process for this article was delegated to GP.

Appendix

To assess the influence of the signal-to-noise ratio (SNR) in the relations between different parts of mAP we have mixed different degrees of known noise ($n_{i,}$, $i = 1, 2, \ldots N$) with the numerical model of mAP ($s_{i,}$, $i = 1, 2, \ldots N$). The definition of SNR is given as

$$SNR = 10 \log_{10} \frac{\sum_{i=1}^{N} s_i^2}{\sum_{i=1}^{N} n_i^2}$$

We have simulated a P1N1 mAP fitting the next properties (i) two opposite phases of depolarization followed by repolarization, (ii) $V_{Dep} = 1.63 \times |V_{Rep}|$ and v) $d_{Dep} \sim 0.38 d_{Rep}$. We were not interested in properties (iii) and (iv) related to dV_{max} and therefore they have not been modeled.

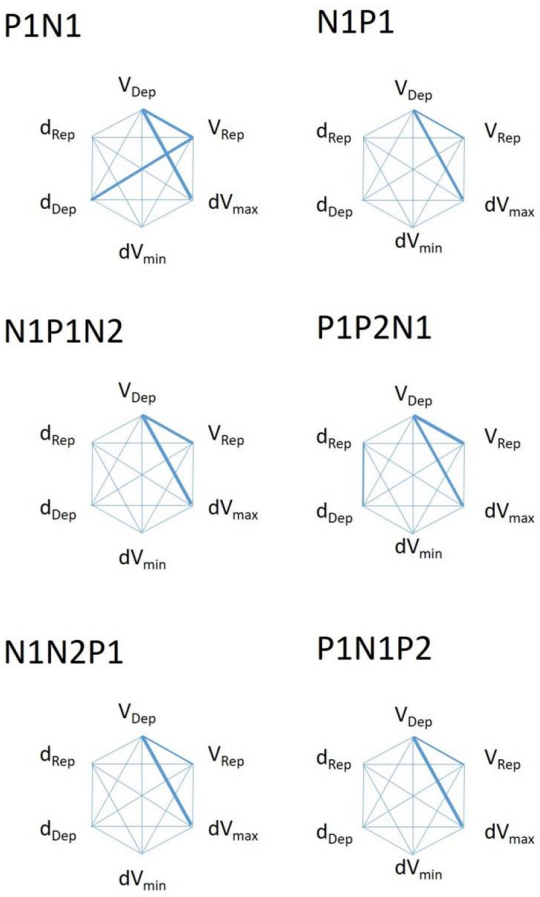

Fig. 7. Network plot for correlations between variables for all the kind of mAP. The strength of correlation is indicated by the thickness of line.

To simulate noise, we have chosen a function like this $n(t) = A \sin(2\pi f t + \varphi)$, with amplitude (A) and phase (φ) random and $f = 1920\ Hz$. We have performed 7 simulations, with the first without noise. Every simulation included 30 repetions with a random phase. The probability density function for all repetitions fitted well to Gaussian distribution by effect of the random phase. For the resulted waveform (mAP + noise) we determined the fiducial points (Appendix Fig. 8).

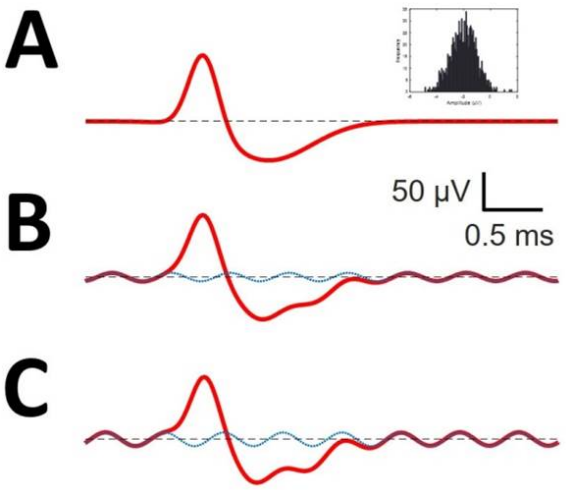

Fig. 8. Different mixtures of the model of mAP with noise. (A) Signal without noise. (B) SNR = 17.1, A = 5.2 μV. (C) SNR = 12.7, A = 8.6 μV. Red = waveform resulting from numerical model of mAP + noise; dotted blue = high frequency noise; dashed black = basal zero-voltage. Inset: bar histrogram for an overall analysis of 30 repetitions.

We have plotted these results at Appendix Fig. 8. We can observe that there was a very good correlation between A and V_{Dep}, V_{Rep} and d_{Dep}, but not with d_{Rep}. Besides, it was a very good correlation between V_{Dep} vs V_{Rep} and between V_{Dep} vs d_{Dep}, but not between d_{Dep} vs d_{Rep} or V_{Rep} vs d_{Rep}. Interestingly the V_{mAP} did not correlate with A, because, in fact, can be considered as constant independent of noise, at least for a SNR between 33.5 (A = 0.8 μV) and 7.1 (A = 16.3 μV). However, although d_{mAP} was not correlated with A, cannot be considered as a constant.

But, not only no correlation between durations were obtained, besides the coefficient of variation was higher for d_{Dep}/d_{Rep} (0.266) than for V_{Dep}/V_{Rep} (0.153), what mean that noise increase the dispersion for measurement of duration.

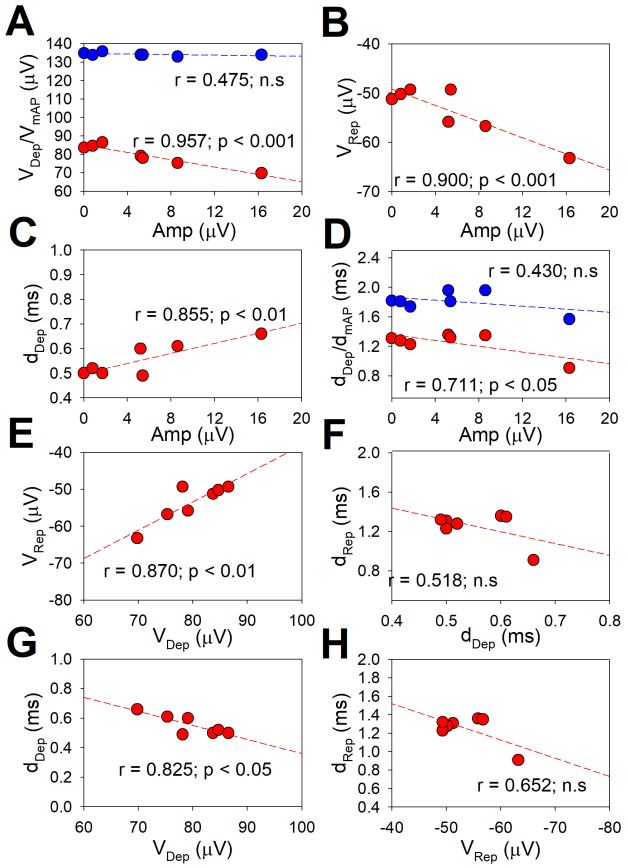

Fig. 9. Relationships between variables from different mixtures of mAP + noise. (A) A vs V_{Dep} (red dots) and A vs V_{mAP} (blue dots) (B) A vs V_{Rep} (C) A vs d_{Dep} (D) A vs d_{Dep} (red dots) and A vs d_{mAP} (blue dots) (E) V_{Dep} vs V_{Rep} (F) d_{Dep} vs d_{Rep} (G) V_{Dep} vs d_{Dep} (H) V_{Rep} vs d_{Rep}. Dashed lines are regression functions. Values of r and statistical significance (*p*) for every regression function are indicated. Vertical error bars inside the symbols.

References

[1] Pastor J, Vega-Zelaya L. Can we put aside microelectrode recordings in Deep Brain Stimulation surgery? Brain Sciences. 2020; 10: 571.

[2] Sano K, Mayanagi Y, Sekino H, Ogashiwa M, Ishijima B. Results of stimulation and destruction of the posterior hypothalamus in man. Journal of Neurosurgery. 1970; 33: 689–707.

[3] Sano K, Mayanagi Y. Posteromedial Hypothalamotomy in the Treatment of Violent, Aggressive Behaviour. Personality and Neurosurgery. 1988; 37: 145–151.

[4] Franzini A, Marras C, Ferroli P, Bugiani O, Broggi G. Stimulation of the Posterior Hypothalamus for Medically Intractable Impulsive and Violent Behavior. Stereotactic and Functional Neurosurgery. 2005; 83: 63–66.

[5] Franzini A, Messina G, Cordella R, Marras C, Broggi G. Deep brain stimulation of the posteromedial hypothalamus: indications, long-term results, and neurophysiological considerations. Neurosurgical Focus. 2010; 29: E13.

[6] Hernando V, Pastor J, Pedrosa M, Peña E, Sola RG. Low-Frequency Bilateral Hypothalamic Stimulation for Treatment of Drug-Resistant Aggressiveness in a Young Man with Mental Retardation. Stereotactic and Functional Neurosurgery. 2008; 86: 219–223.

[7] Torres CV, Sola RG, Pastor J, Pedrosa M, Navas M, García-Navarrete E, *et al*. Long-term results of posteromedial hypothalamic deep brain stimulation for patients with resistant aggressiveness. Journal of Neurosurgery. 2013; 119: 277–287.

[8] Nieuwenhuys R, Voogd J, Van Huijzen C. The Human Central Nervous System (pp. 289–323). 4th edn. Springer: New York. 2008.

[9] Heinricher MM. Microelectrode Recording in Movement disorder surgery (pp. 8–13). 1st edn. Thieme: New York. 2004.

[10] Obwegeser AA, Uitti RJ, Turk MF, Strongosky AJ, Wharen RE. Thalamic stimulation for the treatment of midline tremors in essential tremor patients. Neurology. 2000; 54: 2342–2344.

[11] Wu D, Wang S, Stein JF, Aziz TZ, Green AL. Reciprocal interactions between the human thalamus and periaqueductal gray may be important for pain perception. Experimental Brain Research. 2014; 232: 527–534.

[12] Li X, Zhuang P, Hallett M, Zhang Y, Li J, Li Y. Subthalamic oscillatory activity in parkinsonian patients with off-period dystonia. Acta Neurologica Scandinavica. 2016; 134: 327–338.

[13] Alam M, Sanghera MK, Schwabe K, Lütjens G, Jin X, Song J, *et al*. Globus pallidus internus neuronal activity: a comparative study of linear and non-linear features in patients with dystonia or Parkinson's disease. Journal of Neural Transmission. 2016; 123: 231–240.

[14] Messina G, Islam L, Cordella R, Gambini O, Franzini A. Deep brain stimulation for aggressive behavior and obsessive-compulsive disorder. Journal of Neurosurgical Sciences. 2016; 60: 211–217.

[15] Pastor J, Vega-Zelaya L, Martín Abad E. Properties of extracelular action potentials from posteromedial hypothalamus. Clinics in Surgery. 2021; 6: 3224.

[16] Vega-Zelaya L, Torres CV, Navas M, Pastor J. Neurophysiological characterization of thalamic nuclei in anaesthetized patients. Brain Sciences. 2019; 9: 312.

[17] Galazky I, Kaufmann J, Voges J, Hinrichs H, Heinze HJ, Sweeney-Reed CM. Neuronal spiking in the pedunculopontine nucleus in progressive supranuclear palsy and in idiopathic Parkinson's disease. Journal of Neurology. 2019; 266: 2244–2251.

[18] Weinberger M, Hamani C, Hutchison WD, Moro E, Lozano AM, Dostrovsky JO. Pedunculopontine nucleus microelectrode recordings in movement disorder patients. Experimental Brain Research. 2008; 188: 165–174.

[19] Pastor J, Vega-Zelaya L. Features of action potentials from identified thalamic nuclei in anesthetized patients. Brain Sciences. 2020; 10: 1002.

[20] Pastor J, Vega-Zelaya L, Martin Abad, E. Neurophysiological Characterization of Posteromedial Hypothalamus in Anaesthetized Patients. Brain Sciences. 2022; 12: 43.

[21] Micieli R, Rios ALL, Aguilar RP, Posada LFB, Hutchison WD. Single-unit analysis of the human posterior hypothalamus and red nucleus during deep brain stimulation for aggressivity. Journal of Neurosurgery. 2017; 126: 1158–1164.

[22] Hassler R. Introduction to stereotaxis with an atlas of the human brain (pp. 230–290). 1st edn. Thieme: New York. 1959.

[23] Blasco García de Andoain G, Navas García M, González Aduna Ó, Bocos Portillo A, Ezquiaga Terrazas E, Ayuso-Mateos JL, *et al*. Posteromedial Hypothalamic Deep Brain Stimulation for Refractory Aggressiveness in a Patient with Weaver Syndrome: Clinical, Technical Report and Operative Video. Operative Neurosurgery. 2021; 21: 165–171.

[24] Pastor J, Vega-Zelaya L. A new potential specifically marks the sensory thalamus in anaesthetized patients. Clinical Neurophysiology. 2019; 130: 1926–1936.

[25] Van Drongelen W. Signal Processing for Neuroscientists (pp. 205–217). 1 st edn. Elsevier: Amsterdam. 2007.

[26] Peña D, Prieto FJ. The kurtosis coefficient and the linear discriminant function. Statistics & Probability Letters. 2000; 49: 257–261.
[27] Spiegel MR, Schiller J, Srinivasan RA. Probabilidad y Estadística. McGraw-Hill: Bogotá. 2003.
[28] Gold C, Henze DA, Koch C, Buzsáki G. On the Origin of the Extracellular Action Potential Waveform: a Modeling Study. Journal of Neurophysiology. 2006; 95: 3113–3128.
[29] Henze DA, Borhegyi Z, Csicsvari J, Mamiya A, Harris KD, Buzsáki G. Intracellular Features Predicted by Extracellular Recordings in the Hippocampus in Vivo. Journal of Neurophysiology. 2000; 84: 390–400.
[30] Galazky I, Kaufmann J, Lorenzl S, Ebersbach G, Gandor F, Zaehle T, *et al*. Deep brain stimulation of the pedunculopontine nucleus for treatment of gait and balance disorder in progressive supranuclear palsy: Effects of frequency modulations and clinical outcome. Parkinsonism & Related Disorders. 2018; 50: 81–86.
[31] Shimamoto SA, Larson PS, Ostrem JL, Glass GA, Turner RS, Starr PA. Physiological identification of the human pedunculopontine nucleus. Journal of Neurology, Neurosurgery & Psychiatry. 2010; 81: 80–86.
[32] Johnston D, Miao-Sin Wu S. Foundations of cellular Neurophysiology. The MIT Press: Massachusetts. 1995.
[33] Baker PF. The Biophysical Basis of Excitability. FEBS Letters. 1985; 208: 171–171.
[34] Dayan P, Abbot LF. Theoretical Neuroscience. The MIT Press: Massachusetts. 2001.
[35] Holt GR, Koch C. Electrical Interactions via the Extracellular Potential near Cell Bodies. Journal of Computational Neuroscience. 1999; 6: 169–184.
[36] Dumitru D. Volume conduction (pp. 29–65). Hanley & Belfus: Philadelphia. 1995.
[37] Bakkum DJ, Obien MEJ, Radivojevic M, Jäckel D, Frey U, Takahashi H, *et al*. The Axon Initial Segment is the Dominant Contributor to the Neuron's Extracellular Electrical Potential Landscape. Advanced Biosystems. 2019; 3: 1800308.
[38] Anastassiou CA, Perin R, Buzsáki G, Markram H, Koch C. Cell type- and activity-dependent extracellular correlates of intracellular spiking. Journal of Neurophysiology. 2015; 114: 608–623.
[39] Gold C, Girardin CC, Martin KAC, Koch C. High-Amplitude Positive Spikes Recorded Extracellularly in Cat Visual Cortex. Journal of Neurophysiology. 2009; 102: 3340–3351.
[40] Koester J, Siegelbaum SA. Membrane Potential. In Principles of Neural Science. 5th edn. Mc. Graw Hill: New York. 2014.
[41] Nagy JI, Patel D, Ochalski PAY, Stelmack GL. Connexin30 in rodent, cat and human brain: selective expression in gray matter astrocytes, co-localization with connexin43 at gap junctions and late developmental appearance. Neuroscience. 1999; 88: 447–468.
[42] Sutor B. Gap Junctions and their Implications for Neurogenesis and Maturation of Synaptic Circuitry in the Developing Neocortex. Results and Problems in Cell Differentiation. 2002; 68: 53–73.
[43] Hatch RJ, Mendis GDC, Kaila K, Reid CA, Petrou S. Gap Junctions Link Regular-Spiking and Fast-Spiking Interneurons in Layer 5 Somatosensory Cortex. Frontiers in Cellular Neuroscience. 2017; 11: 204.
[44] Simms BA, Zamponi GW. Neuronal voltage-gated calcium channels: structure, function, and dysfunction. Neuron. 2014; 82: 24–25.